Available online at www.sciencedirect.com
SCIENCE DIRECT®
Journal of Power Sources 117 (2003) 260–266
JOURNAL OF POWER SOURCES
www.elsevier.com/locate/jpowsour

Correlation between charge input and cycle life of MgNi electrode for Ni–MH batteries

Stéphane Ruggeri, Lionel Roué*

INRS-Énergie et Matériaux, 1650 Boulevard Lionel-Boulet, C.P. 1200 Varennes, Que., Canada J3X 1S2

Received 14 January 2003; accepted 31 January 2003

Abstract

Amorphous MgNi material has been prepared by mechanically alloying magnesium and nickel powders for 10 h. Its cycle life as a negative electrode for nickel–metal hydride (Ni–MH) batteries has been studied with charge inputs varying from 0 to 600 mAh/g. For charge inputs lower than 400 mAh/g, the first cycle discharge capacity is superior to the charge input capacity. This surplus discharge capacity can be associated with the alloy oxidation to $Mg(OH)_2$ and $Ni(OH)_2$. For charge inputs higher than 400 mAh/g, the initial discharge capacity becomes inferior to the charge input capacity due to the progressive decrease of the charge efficiency related to the hydrogen evolution side reaction. From the second charge/discharge cycle, no additional discharge capacity appears and no discharge capacity degradation occurs for charge inputs inferior or equal to 233 mAh/g. In contrast, for higher charge input values, an important decay in the discharge capacity appears, which is accentuated with increasing charge input. The thresholds charge input of 233 mAh/g corresponds to an amount of hydrogen absorbed into the alloy of 0.8 wt.% ($MgNiH_{0.7}$). For higher absorbed hydrogen amounts, it is assumed that extended electrode pulverization occurs, which breaks the passive surface layer of $Mg(OH)_2$ formed during the first charge/discharge cycle. This creates unprotected fresh MgNi surfaces and consequently, leads to electrode capacity degradation. The stability of the MgNi electrode for absorbed hydrogen content lower than 0.8 wt.% may be related to its amorphous character, which favors a gradual volume expansion upon hydrogen absorption in contrast to crystalline compounds characterized by an abrupt α-to-β lattice expansion.

Keywords: Nickel–metal hydride battery; Hydrogen storage alloys; Magnesium-based compounds; Mechanical alloying; Cycle life

1. Introduction

Rapid advance in portable electronic technologies and increasing interest in the electric vehicles (EVs) have stimulated research efforts to develop high-performance rechargeable batteries. During the 1990s, the nickel–metal hydride (Ni–MH) technology received much attention because of its performance, safety and environmental friendliness. Presently, the majority of the Ni–MH battery manufacturers utilize $LaNi_5$-based alloys as negative electrode materials. These metal hydrides are multicomponent systems with a composition such as $(Mm)(Ni–Co–Mn–Al)_5$ where Mm is a naturally occurring mixture of rare earths (La, Ce, Nd, Pr). The various substituents for La and Ni stabilize the electrode during charge/discharge cycling by reducing the alloy expansion and/or forming protective surface films. However, such materials have the disadvantage of being expensive. In addition, higher power density MH electrodes are needed for targeting the emerging EV and hybride electric vehicle (HEV) market.

Promising results have recently been obtained with inexpensive Mg–Ni-based alloys prepared by mechanical alloying. These materials typically have a capacity of 400–500 compared to 250–300 mAh/g for $LaNi_5$-based alloys. However, the low cycle lifetime of Mg-based electrodes, typically a few cycles compared to several hundreds of cycles for $LaNi_5$-based electrodes, limits their commercial use. The capacity degradation is associated with the irreversible oxidation of the Mg-based alloy by the electrolyte (concentrated KOH) leading to the formation of a $Mg(OH)_2$ layer on the surface of the alloy particles [1–8]. This consumes active material, affects the charge transfer across the alloy/electrolyte interface and may act as a barrier for hydrogen diffusion into and from the alloy.

In the last few years, several studies have been conducted to increase the cycle life of Mg-based electrodes by three ways: the first one is to adjust the composition of the MgNi materials by substitution of certain elements for Mg and/or

* Corresponding author. Tel.: +1-450-929-8100; fax: +1-450-929-8102.
E-mail address: roue@inrs-ener.uquebec.ca (L. Roué).

0378-7753/03/$ – see front matter © 2003 Elsevier Science B.V. All rights reserved.
doi:10.1016/S0378-7753(03)00355-0

Ni; the second one is to form composite material by additional compounds or elements and the last one consists of modifying the surface of the alloys by chemical treatment or by electroless and electrochemical deposits. Up till now, the most promising results have been obtained by partial substitution methodology. For example, amorphous $Mg_{0.7}Ti_{0.3}Ni$ alloy retains 92% of its initial discharge capacity of 325 mAh/g after 20 cycles [9]; the discharge capacity of $Mg_{1.95}Y_{0.05}Ni_{0.92}Al_{0.08}$ nanocrystalline alloy electrode decays to about 98% of the initial capacity (380 mAh/g) after 150 cycles [10]. However, the global performance of such improved Mg-based electrodes is still far from that required for commercial application.

The common approach in the above-mentioned methodologies for increasing the cycle life of Mg-based electrodes is to improve the alloy oxidation resistance. In the present study, it will be demonstrated that the continuous discharge capacity decay of the MgNi electrode upon cycling can be prevented, without modifying its composition, but through strict control of the electrode charge input.

2. Experimental

Amorphous MgNi material was prepared by mechanical alloying of magnesium and nickel powders for 10 h, with a ball-to-powder mass ratio of 10:1, using a SPEX 8000 miller. The amorphous structure of the end product was confirmed by X-ray diffraction analysis. Scanning electron microscopy observations indicated that the alloy powders consist of irregular particles with a grain size distribution varying from less than 1 μm to several tens of micrometer. The mean particle size was estimated at ca. 1 μm.

The electrochemical charge/discharge cycling tests were performed on an Arbin BT2000 battery tester at room temperature ($23 \pm 1\ ^{\circ}C$) in a 6 M KOH solution using a three-electrode cell. The working electrode was a compacted mixture of 100 mg of active material and 800 mg of graphite, plus 20 mg of carbon black. The electrode was vacuum impregnated with electrolyte for few minutes before cycling in order to start with a completely wetted internal surface. The counter electrode was made of a nickel wire and the reference electrode was an Hg/HgO electrode (XR440 from Radiometer). The electrodes were charged at −200 mA/g for different durations varying from 0 to 180 min. Discharges were performed at 20 mA/g to −0.4 V versus Hg/HgO electrode after resting for 5 min.

Cyclic voltammetry experiments on MgNi electrode (consisting of 1 g of pure active material) were carried out at 0.5 mV/s in 6 M KOH solution from open circuit potential to −0.4 V versus Hg/HgO using a Voltalab40 (Radiometer Analytical) potentiostat/galvanostat/FRA apparatus. No cathodic polarization and short immersion period (5 min) in open circuit conditions were done before starting the experiment in order to avoid any anodic current related to the hydrogen desorption reaction.

3. Results and discussion

The cycle discharge behavior of MgNi electrode for different charge inputs is presented in Fig. 1. Some characteristic values such as the initial discharge capacity, the cycling capacity retention after 15 cycles (C_{15}/C_1) and between the 2nd and the 15th cycle (C_{15}/C_2) versus the charge inputs, varying from 0 to 600 mAh/g, are reported in Table 1.

As shown in Fig. 1, the first cycle discharge capacity is superior to the charge input capacity when the charge input is less or equal to 333 mAh/g. This is more evident in Fig. 2, in which the difference between the initial discharge capacity of MgNi electrode and the charge input ($\Delta C = C_1 - C_{input}$) is plotted as a function of the charge input. It appears that the additional charge increases almost linearly with increasing charge input up to a maximum value of 109 mAh/g for a charge input of 233 mAh/g. For higher charge input values, a linear decrease of ΔC is observed and it becomes even negative for $C_{input} = 400$ mAh/g.

The additional discharge capacity could be related to the well-known irreversible reaction:

$$MgNi + 2OH^- \rightarrow Mg(OH)_2 + Ni + 2e^- \quad (1)$$

and to the possible subsequent reaction:

$$Ni + 2OH^- \rightarrow Ni(OH)_2 + 2e^- \quad (2)$$

The formation of $Mg(OH)_2$, Ni and $Ni(OH)_2$ upon cycling was confirmed by XRD and XPS analyses [8].

The increasing additional discharge capacity with charge input can be explained by the accentuation of the decrepitation of MgNi particles due to their volume expansion increasing with absorbed hydrogen content. The electrode pulverization creates new fresh surfaces susceptible to oxidation and consequently raises the additional anodic charge associated with the $Mg(OH)_2$ and $Ni(OH)_2$ formation. However, for charge input values higher than 233 mAh/g, one observes a linear decreasing of the surplus discharge capacity, which becomes a deficient capacity ($\Delta C < 0$) from $C_{input} \approx 400$ mAh/g. This does not preclude the presence of an anodic current related to the $Mg(OH)_2$ and $Ni(OH)_2$ formation, which may be overshadowed by the progressive decrease of the charge efficiency related to the concomitant hydrogen evolution reaction (HER) accentuated with prolonged charge conditions. HER is confirmed by the appearance of bubbles of gas from the working electrode as well as the stabilization of the charge potential around −1.07 V versus Hg/HgO, as indicated in Fig. 3, which compares the charge curves for a charge input of 233 mAh/g (no HER) and for a charge input of 466 mAh/g (HER occurrence).

In addition, when the electrode is left in KOH solution at open circuit potential (∼−0.65 V versus Hg/HgO) during 24 h before charging, the surplus discharge capacity is less important (e.g. 70 compared to 109 mAh/g for a charge input of 233 mAh/g). This indicates that the magnesium hydroxide film is formed in open circuit conditions, but because

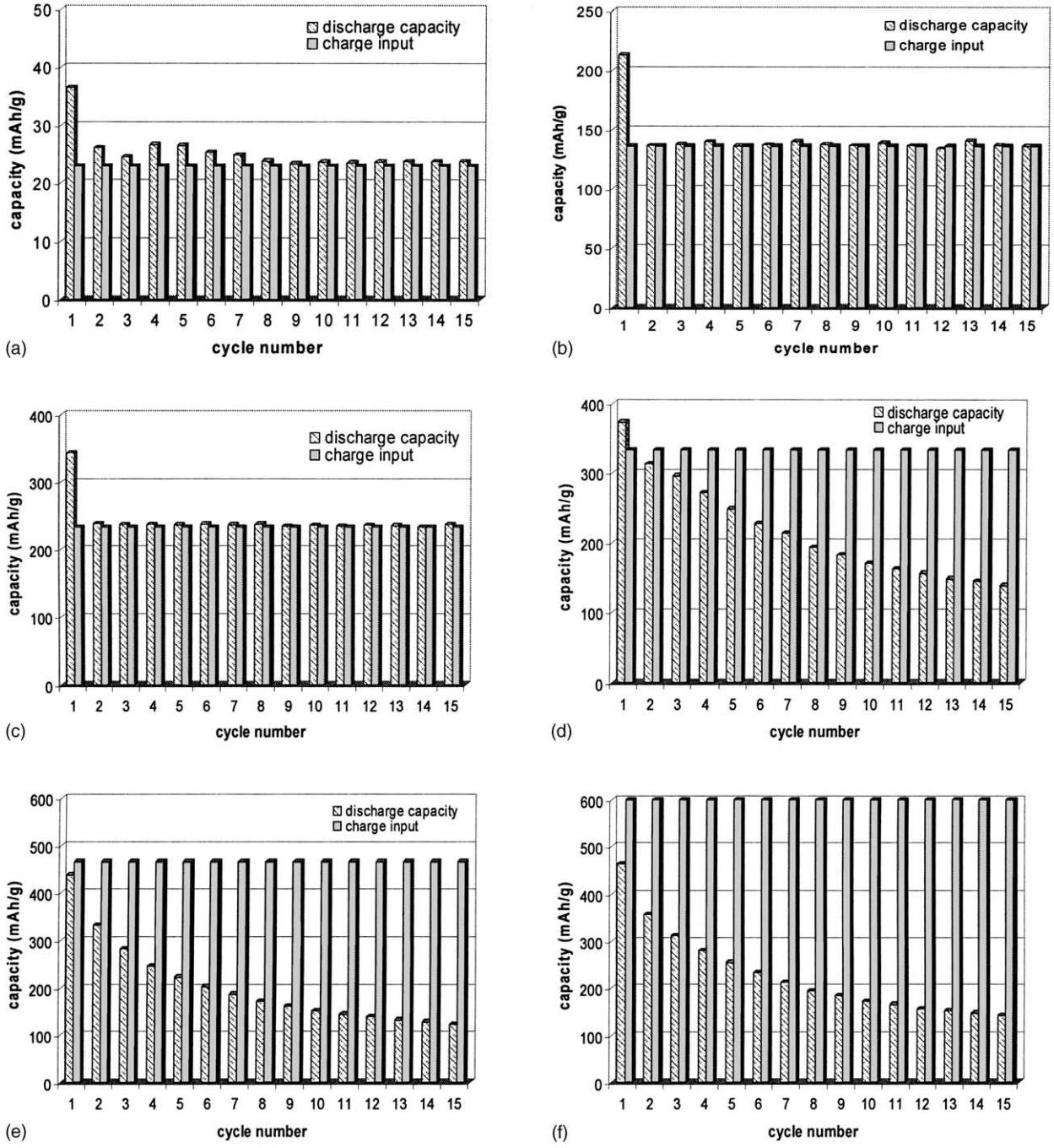

Fig. 1. Cycle life plots of MgNi electrode for various charge inputs: (a) 23 mAh/g; (b) 136 mAh/g; (c) 233 mAh/g; (d) 333 mAh/g; (e) 466 mAh/g; (f) 600 mAh/g (f).

Table 1
Cycling discharge capacities of MgNi electrode for different charge inputs

Charge input (mAh/g)	C_1 (mAh/g)	C_2 (mAh/g)	C_{15} (mAh/g)	C_{15}/C_2 (%)	C_{15}/C_1 (%)
0	5	–	–	–	–
23	37	26	26	100	70
136	213	136	136	100	64
233	342	238	238	100	70
333	373	312	138	44	37
466	437	332	123	37	28
600	465	356	142	40	30

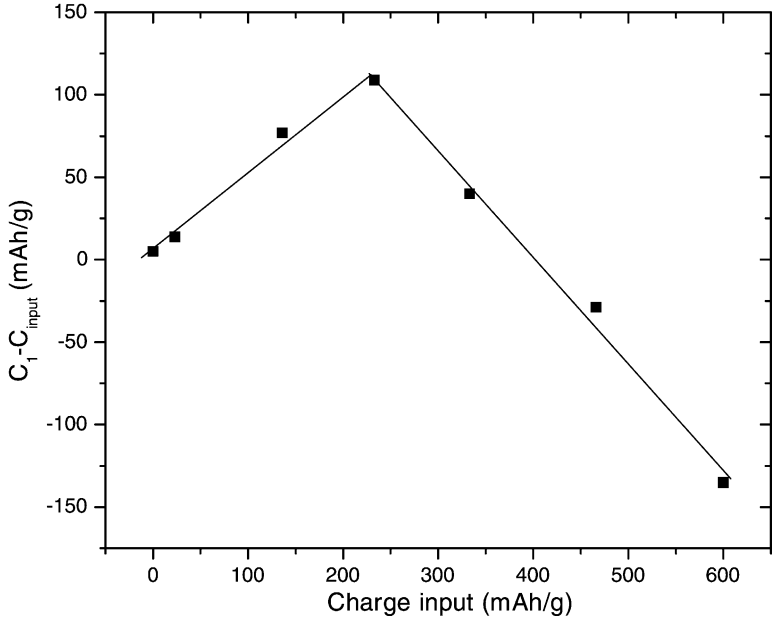

Fig. 2. Difference between the initial discharge capacity of MgNi electrode and the charge input ($\Delta C = C_1 - C_{input}$) as a function of the charge input.

additional discharge capacity is still present, this tends to confirm that the charge procedure, through the pulverization process, creates new surfaces to be oxidized.

On the other hand, from the second charge/discharge cycle and for charge input inferior or equal to 233 mAh/g, the discharge capacity is equal to the charge input, i.e. no additional discharge capacity appears and no discharge capacity degradation occurs. This reflects two major aspects:

(i) The $Mg(OH)_2$ layer formed on MgNi particles during the first cycle protects the electrode against further corrosion reaction. This can be related to the passivating character of the magnesium hydroxide film formed at the surface of the alloy particles. This passive behavior is confirmed in Fig. 4, which shows successive cyclic voltammograms for uncharged MgNi electrode performed from open circuit potential to −0.4 V versus Hg/HgO (i.e. in the discharge potential range). During the first cycle, it appears a large anodic current associated with the $Mg(OH)_2$ and $Ni(OH)_2$ formation. This anodic current decreases progressively during the subsequent cycles and after six cycles, a

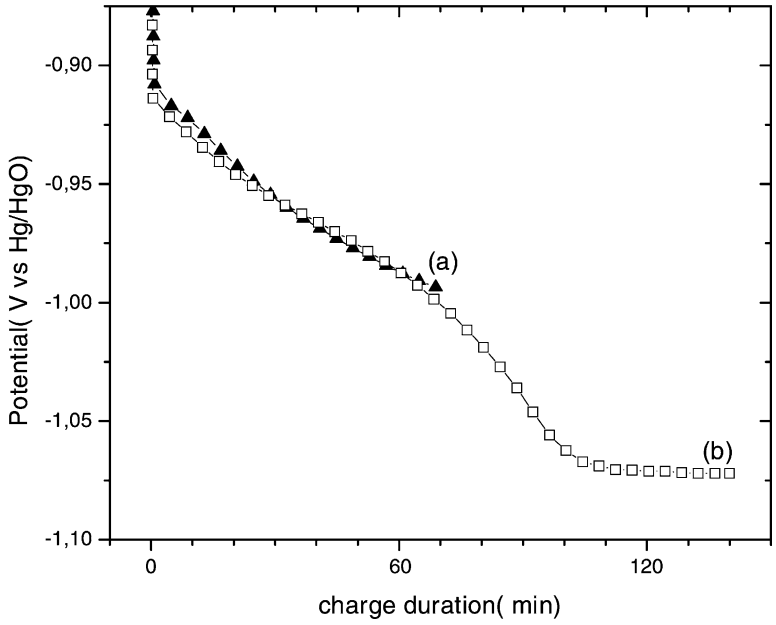

Fig. 3. Typical charge curves of MgNi electrode for a charge input of (a) 233 mAh/g and (b) 466 mAh/g.

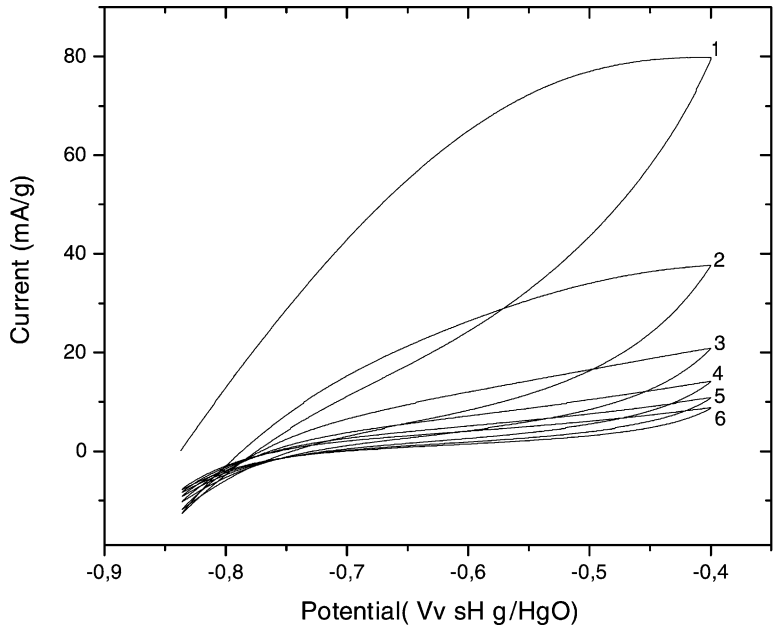

Fig. 4. Successive cyclic voltammograms for uncharged MgNi electrode in 6 M KOH.

nearly stabilized voltammogram is observed with a characteristic potential independent passive current.

(ii) Fresh surfaces are not created from the second cycle. In other words, electrode decrepitation occurs essentially during the first cycle and is prevented during the following charge/discharge cycles when the charge input is limited to 233 mAh/g.

In contrast, as shown in Fig. 1, an important decay in the discharge capacity appears for charge inputs higher than 233 mAh/g and the capacity decay is accentuated with increasing charge input, i.e. the discharge capacity evolution with the cycle number changes from a nearly linear decay for a charge input of 333 mAh/g to an increasingly marked exponential decay for higher charge input values. The accentuation of the capacity loss with increasing charge input is clearly apparent in Fig. 5, which shows that the discharge capacity loss between the 2nd and the 15th cycle ($\Delta C = C_2 - C_{15}$) is non-existent for charge inputs below or equal to 233 mAh/g; loss increase is abrupt for higher charge

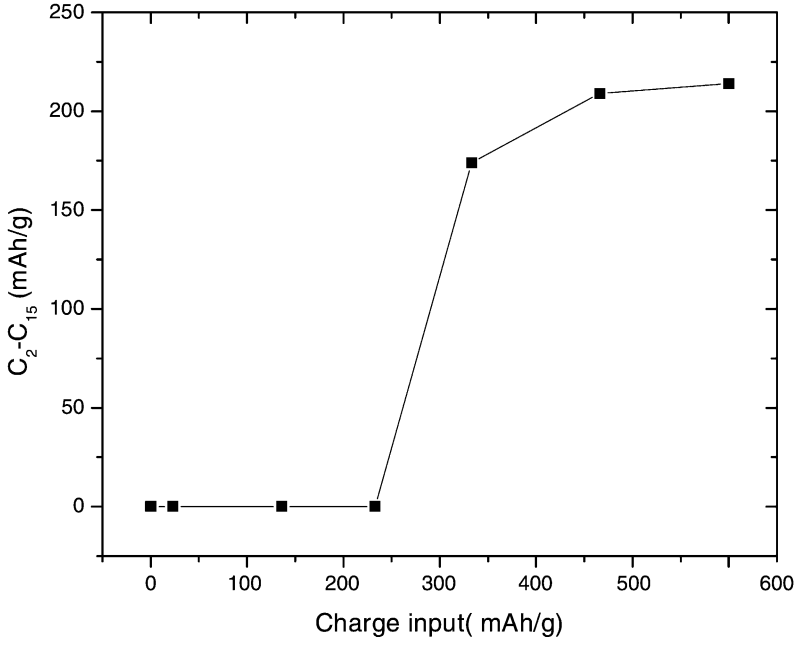

Fig. 5. Discharge capacity loss of MgNi electrode between the 2nd and the 15th charge/discharge cycle ($\Delta C = C_{15} - C_2$) as a function of the charge input.

inputs values and tends to stabilize at ca. 210 mAh/g for charge inputs above or equal to 466 mAh/g.

Assuming that during a charge input of 233 mAh/g, all of the charge current is consumed in the hydrogen absorption reaction and considering that the maximum discharge capacity of MgNi electrode is 465 mAh/g (see Table 1), the charge input of 233 mAh/g is equivalent to a state of charge (SOC) of the MgNi electrode equal to 50% and it corresponds to hydrogen content of 0.8 wt.% (i.e. $MgNiH_{0.7}$). Based on the present observations, this is the maximum amount of hydrogen that the Mg–Ni alloy can absorb without capacity degradation from the second charge/discharge cycle. For higher absorbed hydrogen amounts, it is assumed that extended electrode pulverization occurs, which breaks the passive surface layer of $Mg(OH)_2$ formed during the first charge/discharge cycle, creates unprotected fresh MgNi surfaces and consequently, leads to the electrode capacity decay.

Furthermore, the cycle life curves in Fig. 1 are re-plotted in Fig. 6 as a function of immersion time in KOH electrolyte (i.e. sum of charge/discharge times plus open circuit periods). No clear relation can be established between the immersion duration and the capacity decay rate. This confirms that the calendar corrosion is not the main degradation process. This result is in contradiction with the study of Hatano et al. [5], indicating that the degradation rate of the Mg–Ni alloy in the charge/discharge cycle test is comparable to that induced by the alkaline immersion under open circuit potential.

Actually, the mechanism of the MgNi capacity degradation is close to that assumed for AB_5 compounds. Willems [11] demonstrated that the capacity decrease of $LaNi_5$-based electrodes for Ni–MH batteries was attributed to the decomposition of the alloy through the formation of $La(OH)_3$ and 3d transition metal precipitates by contact with the electrolyte. This corrosion process was directly related to the expansion and shrinkage of the intermetallic compound particles during charging and discharging process. The volume expansion was estimated to be 20% and more during hydriding, which induced an enormous mechanical stress into the alloy. Disintegration of the particles into smaller fragments was observed, creating new fresh surfaces susceptible to corrosion. Moreover, the mechanical stress (concentrated at the hydrogen-poor α/hydrogen-rich β phase boundary) would diminish the activation energy for diffusion of lanthanum, inducing a zone of enhanced mobility through the particles and consequently enabling the transport of La to the surface and its further oxidation by electrolyte. The stability improvement of the electrode capacity in proportion to the decreasing volume expansion was clearly demonstrated through the comparison of various $LaNi_5$-related compounds. Later, Notten et al. demonstrated from in situ XRD investigations on AB_5 alloys that the discrete α-to-β lattice expansion rather than the total lattice expansion is responsible for the particle cracking. In contrast, AB_6 material lacking an α–β phase transition region is much more resistant to pulverization [12]. In the same way, because of the amorphous structure of Mg–Ni alloy, no abrupt α-to-β phase transition occurs, as might be expected from its hydrogen pressure–composition isotherm [13], which showed a sloping plateau in comparison to the flat plateau characteristic of crystalline hydrogen storage alloys. Consequently, the mechanical stress related to volume expansion upon hydrogen absorption is expected to be lower and more progressive than for the crystalline $LaNi_5$ alloy and this can explain the stability of the MgNi

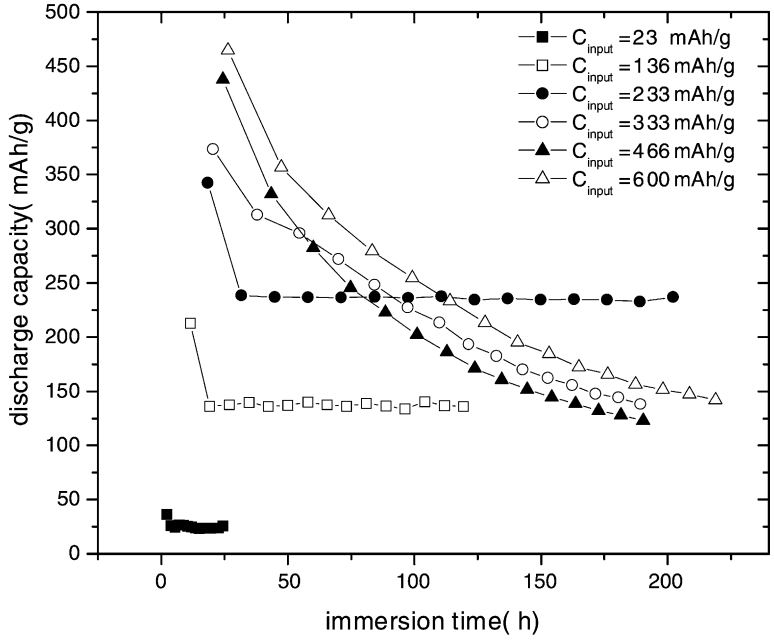

Fig. 6. Cycle life plots of MgNi electrode with immersion time for various charge inputs.

discharge capacity for absorbed hydrogen content lower than 0.8 wt.%.

On the other hand, Willems [11] reported from BET measurements of $LaNi_5$ powder as a function of the number of gas cycles that cracking mainly occurred during the first 50 cycles and that particle size aimed at a limiting value of 2–3 μm. More recently, Geng et al. [14] estimated from electrochemical measurements of hydrogen diffusivities that the radius of the $LaNi_{4.7}Al_{0.3}$ alloy particles was about 7.7 μm after the first charge/discharge cycle and decreased to about 3.3 μm after 20 cycles and 2.8 μm after 45 cycles. Thus, because of the initial mean size of the MgNi particles is as low as 1 μm, their fragmentation upon cycling is expected to be less extended than for large $LaNi_5$ particles and it is not surprising that it occurs mainly during the first cycle.

BET surface area measurements of the MgNi powder before and after cycling was performed in order to quantify the powder cracking. However, the increase in surface area related to particle pulverization was overshadowed by the high surface area of the oxidation products formed onto the MgNi powder during electrochemical test and consequently, pulverization quantification was impossible. In parallel, hydrogen absorption/desorption cycles were performed in the gas phase, but the high temperature (300 °C) required to desorb hydrogen from the alloys led to their crystallization and consequently, the subsequent BET surface area measurements were also altered. In addition, scanning electron microscopy observations of the electrode powder before and after electrochemical cycling as well as in situ atomic force microscopy study did not permit a precise quantification of the powder decrepitation. Additional studies are in progress to quantify the volume expansion of Mg–Ni alloy followed hydrogen absorption by in situ XRD experiments.

4. Conclusion

The influence of the charge input value on the discharge behavior of MgNi electrodes has been studied. It was demonstrated that the cycle life of the MgNi electrode can be drastically extended by a strict control of the electrode charge input. The essential cause of the capacity degradation during charge/discharge cycles is not the corrosion but rather the electrode pulverization which is accentuated greatly when the charge input is higher than 233 mAh/g. This threshold value corresponds to a hydrogen content into the alloy of 0.8 wt.% ($MgNiH_{0.7}$). For lower hydrogen contents, the level of mechanical stress into the particles related to their volume expansion is assumed to be low and no continuous decrepitation occurs. Consequently, the passive $Mg(OH)_2$ surface layer formed onto the MgNi particles during the first cycle is not broken and can maintain its protective function against further corrosion. This study demonstrates that the key issue to obtain a stable Mg-based electrode is to limit its decrepitation by decreasing its volume expansion and by improving its mechanical properties (resistance to rupture). For that purpose, experiments to quantify the pulverization and the volume expansion of MgNi-related alloys as a function of their composition and their hydrogen content are planned.

Acknowledgements

This work has been financially supported by the National Sciences and Engineering Research Council (NSERC) of Canada and the ‘‘Fond de la Recherche sur la Nature et les Technologies’’ of Québec.

References

[1] W. Liu, Y. Lei, D. Sun, J. Wu, Q. Wang, J. Power Sources 58 (1996) 243.
[2] C. Lenain, L. Aymard, J.M. Tarascon, J. Solid State Electrochem. 2 (1998) 285.
[3] N.H. Goo, J.H. Woo, K.S. Lee, J. Alloys Comp. 288 (1999) 286.
[4] C. Lenain, L. Aymard, L. Dupont, J.M. Tarascon, J. Alloys Comp. 292 (1999) 84.
[5] Y. Hatano, T. Tachikawa, D. Mu, T. Abe, K. Watanabe, S. Morozumi, J. Alloys Comp. 330–332 (2002) 816.
[6] T. Abe, T. Tachikawa, Y. Hatano, K. Watanabe, J. Alloys Comp. 330–332 (2002) 792.
[7] D. Mu, Y. Hatano, T. Abe, K. Watanabe, J. Alloys Comp. 334 (2002) 232.
[8] S. Ruggeri, L. Roué, J. Huot, R. Schulz, L. Aymard, J.M. Tarascon, J. Power Sources 112 (2002) 547.
[9] S.C. Han, P.S. Lee, J.Y. Lee, A. Zuttel, L. Schlapbach, J. Alloys Comp. 306 (2000) 219.
[10] N. Cui, J.L. Luo, K.T. Chuang, J. Alloys Comp. 302 (2000) 218.
[11] J.J.G. Willems, Philips J. Res. 39 (1984) 1.
[12] P.H.L. Notten, J.L.C. Daams, R.E.F. Einerhand, J. Alloys Comp. 210 (1994) 233.
[13] S. Ruggeri, L. Roué, G. Liang, J. Huot, R. Schulz, J. Alloys Comp. 343 (2002) 170.
[14] M. Geng, J. Han, F. Feng, D.O. Northwood, J. Electrochem. Soc. 146 (1999) 2371.